Research paper manuscript for publication consideration in

Electrochimica Acta

Re: EA18-5202-R1

Revisiting aqueous redox process of alkyl-linked bis-viologen: Evaluation of redox potential inversion

Takamasa Sagara[a,*], Hitomi Eguchi[b]

[a]*Division of Chemistry and Materials Science, Graduate School of Engineering, Nagasaki University, Bunkyo 1-14, Nagasaki 852-8521, Japan*

[b]*Department of Advanced Engineering, Chemistry and Materials Engineering Program, Graduate School of Engineering, Nagasaki University, Bunkyo 1-14, Nagasaki 852-8521, Japan*

Keywords: bis-viologen; dimerization; two-consecutive one-electron transfer; electroreflectance; ultra-micro electrode

*Corresponding author.

E-mail address: sagara@nagasaki-u.ac.jp (T. Sagara)

Highlights

- Highly water-soluble alkyl-linked bis-viologens were investigated using UME and ER.
- The 2nd reduction potential of butane-1,4-diyl one is 116 mV more positive than the 1st.
- Upon reduction of butane-1,4-diyl one, it completely dimerizes intramolecularly.
- Cf. ethtane-1,2-diyl exhibits repulsive interaction between two viologen sites.

ABSTRACT

Redox reactions of highly water-soluble bis-viologens were examined at Au electrodes using ultra-micro electrode steady state voltammetry and electroreflectance methods in addition to conventional voltammetry. A bulk UV-vis absorption spectral approach was also used. Alkane-1,*n*-diyl bis-viologens appeared as a class of prototypical electroactive molecule possessing two equivalent redox centers; they undergo two-consecutive one-electron transfer processes. When intramolecular dimerization takes place immediately after accepting the second electron to produce a form having two viologen radical cation ($V^{\bullet+}$) sites in one molecule, the second reduction potential may be more positive than the first one. This redox potential inversion is caused by strong tendency to form a stable intramolecular π–π stacking between the two $V^{\bullet+}$ sites. The redox potential inversion of a highly water-soluble bis-viologen with a butane-1,4-diyl linkage was quantitatively obtained to be 116 mV ($E_1 - E_2$ = -116 mV). In contrast, the bis-viologen with an ethane-1,2-diyl linkage exhibited no dimerization below 0.2 mM, and its second redox potential was found to at 63 mV more negative than the first ($E_1 - E_2$ = 63 mV), highlighting repulsive interaction. The value of $E_1 - E_2$ = -116 mV for the bis-viologen with a butane-1,4-diyl linkage corresponds to the attractive interaction energy in the redox process of 5.9 k_BT of room temperature; this value is apparently the same as the dimerization Gibbs free energy of methyl viologen in water.

1. Introduction

Redox reaction of a small molecule possessing two or more equivalent redox sites has been extensively studied so far using multiple-core metal complexes [1] and organic molecules with multi-centers. The electrode reaction model for the two-consecutive one-electron transfer processes of a molecule bearing two-equivalent redox sites is now a textbook knowledge, especially as the E_rE_r reaction when the two one-electron transfer processes are electrochemically reversible [2]. Molecules bearing multiple redox sites are currently drawing much attention because of its importance in electrocatalysis such as oxygen or carbon dioxide reduction, redox splitting of water, and dynamic molecular assembling based on multiple electron transfer processes. One of the focuses of attention is the redox reaction of bis-viologen molecule family [3-17].

A viologen unit, in another name 4,4'-bipyridinium, undergoes stable and fast two-step one-electron transfer processes accompanied by sharp color changes. The one-electron reduction product of a viologen dication (V^{2+}) is a mono-radical mono-cation ($V^{\bullet+}$), and $V^{\bullet+}$ has a strong tendency to form a π-stacked dimer. The second one-electron reduction step produces the neutral quinoid form, V^0. This step is outside the scope of this paper. Focusing exclusively on a bis-viologen molecule bearing two equivalent viologen sites, what follows the two-consecutive one-electron transfer processes is the intramolecular dimerization, $V^{\bullet+}-V^{\bullet+} \rightarrow (V^{\bullet+})_2$, if the molecular structure sterically allows the face-to-face π-stacking. This process has been so far analyzed in depth both electrochemically and spectrophotometrically [3-17]. Bis-viologens found applications to redox-driven molecular tweezers or molecular hinges [11,14,17], a molecular pivot rotation system [12], and a multiple-viologen functionalized transformable dendrimer [15].

When strong tendency to intramolecular dimerization emerges in a bis-viologen molecule, redox potential inversion may be observed so that $E_1 - E_2$ is negative; the redox potential E_1 for the $(V^{\bullet+}-V^{2+})/(V^{2+}-V^{2+})$ redox couple is more negative than the redox potential E_2 for the $(V^{\bullet+}-V^{\bullet+})/(V^{\bullet+}-V^{2+})$ couple. From a thermodynamic viewpoint, this situation is equivalent to the predominant progress of disproportionation reaction of $2(V^{\bullet+}-V^{2+}) \rightarrow (V^{2+}-V^{2+}) + (V^{\bullet+}-V^{\bullet+})$ [1]. In the study on a series of bis-viologens with an alkyl chain linkage, Furue and Nozakura found that a propane-1,3-diyl or longer linkage is needed to realize intramolecular

dimerization [4]. They first quantitatively analyzed dimer formation processes of bis-viologen compounds with alkane-1,*n*-diyl linkage upon reduction in 2-propanol and found also that intramolecular dimerization for $n = 3$ and 4 are the most significant among $n = 2$ through 5.

Redox processes of bis-viologen were further investigated electrochemically. Deronzier and coworkers reported the results of electrochemical measurements of E_1 and E_2 at a Hg electrode in DMF for alkane-1,*n*-diyl bis-viologens and evaluated the potential inversion [5]. Mohammad followed this work in acetonitrile and observed attractive interaction between two $V^{\bullet+}$ units but it was not as much as the level to result in the potential inversion [6]. Neta and coworkers reported not only detailed electrochemical and spectroscopic data for several bis-viologens in water but also kinetic investigation using pulse radiolysis techniques [7]. Lee and coworkers found the formation of a sandwich-type CT complex between a polymethylene-linked bis-viologen as a tetra-cation molecule with 2-naphthol and evaluated an even-odd alternative of the binding energy [8]. We tested the occurrence of a phase transition of butane-1,4-diyl bis-viologen at a HOPG electrode in water but did not mentioned about the intramolecular dimerization in the condensed phase [9]. Asakura and coworkers did not find even dimerization of $V^{\bullet+}$ units in an asymmetric bis-viologen with a butane-1,4-diyl linkage [10].

Redox-activated tweezer, rotatable pivot, and related functions of bis-viologens have been in spotlight. Casellaza and coworkers found that an alkyl-linked bis-viologen of V^0 oxidation state, especially when the linker is octanediyl or nonanediyl, works as a molecular tweezer for fullerene C_{60} [11]. Its open-close is switchable by the redox of the bis-viologen according to their DFT calculation, whereas its affinity to C_{60} in $V^{\bullet+}$ state was not discussed. Iordache and coworkers linked two chemically equivalent viologen sites through a ferrocene pivot and made electrochemical measurements in DMSO [12]. When alkyl linker (methyl or ethyl) was used between ferrocene and viologens, two viologens behaved independently as fully non-interacting centers. In contrast, when alkyne or phenyl rigid linker was used, dimerization of $V^{\bullet+}$ upon reduction triggered the rotation of the ferrocene pivot. Bonchio and coworkers reported a reduction process of an alkyl-linked bis-viologen as a two successive electron transfer followed by slower dimerization step in DMSO [13]. They commented that the dimerization is exclusively an intramolecular process and both enthalpy and entropy changes contribute to the dimerization tendency. Iordache and coworkers reported a bis-porphyrin

pacman-like molecular tweezer driven by propyl linked bis-viologen electroactive hinge [14]. Wadhwa and coworkers synthesized phosphorus-based dendrimer containing six-equivalent terminal viologen units on a hexatopic core [15]. In DMF, reduction to produce six $V^{\bullet+}$ units in a molecule exhibited one CV peak with the peak-to-peak separation of 60 mV. Their voltammetric and spectroscopic data led to a conclusion that, within less than 20 ms, six $V^{\bullet+}$ units in a molecule formed three pairs of intramolecular dimer structures.

Revisiting the fundamentals of electrochemistry of bis-viologen, we aim at precise evaluation of the redox potential inversion, reconfirmation of the occurrence of intramolecular dimerization but not intermolecular one, and spectroelectrochemical approach to support the reaction model. Experiments are conducted in an aqueous medium to provide the data to frequently used aqueous systems, in which viologens play roles as electron shuttles. We have three advanced viewpoints in this work in comparison to the previous reports: (i) the use of highly water-soluble bis-viologen and the choice of electrode, (ii) the use of steady state voltammetry at an ultra-micro electrode (UME), and (iii) the use of electroreflectance (ER) spectroscopy. These are detailed below.

(i) To ensure high water solubility at neutral pH, primary amine groups were attached at the both terminals of alkyl side-chains as shown in Scheme 1. These highly water-soluble bis-viologens are indispensable for the straightforward analysis to exclude complexity due to the precipitation of bis-viologen radical cations, which have lower solubilities than mono-viologen radical cations. Alvarado and coworkers linked two viologen units by *para*-CH_2-Ph-CH_2- to intentionally lower the solubility of its reduced form and not to introduce intramolecular dimerization [16]. Gao and coworkers synthesized bis-viologen type molecular tweezers with a chiral hinge and different linking chain lengths [17]; interestingly, even when all the viologen units were chemically reduced to $V^{\bullet+}$ states in aqueous solution, the presence of the dimeric form was less than 60% while all the dimers were of intramolecular forms. Their electrochemical measurements at a glassy carbon electrode were suffered with strong adsorption of the reduced form.

We had used, at the beginning of this work, bis-viologen compound with a benzyl terminal group but were suffered with both its low solubility and strong adsorption on an electrode surface. The choice of electrode material was another key; a glassy carbon electrode showed a complex ER voltammogram, indicative of adsorption of $V^{\bullet+}$ species even when the

compounds in Scheme 1 were used. In the present work, we used poly-Au electrodes, which, as a result, showed little or no detectable adsorption.

V-C2-V

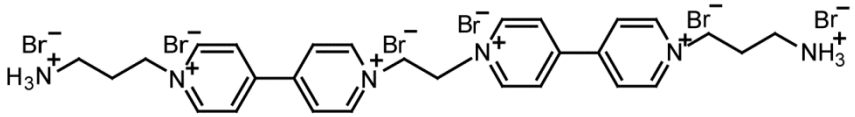

V-C4-V

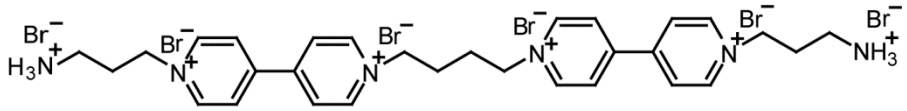

Scheme 1. Bis-viologen compounds used in this work.

(ii) The steady state UME voltammograms exhibited a Nernstian wave at slow potential sweep rates, facilitating us to evaluate E_1 and E_2 in an equilibrium system. Advantages of the use of UME comparing to traditional measurements are that the effect of the ohmic drop is minimized due to small current and that Nernstian relationship is directly figured out, if electrochemically reversible steady-state current-potential curve is obtained [2]. The reversibility can be checked by overlapping of forward and backward scan curves. Then, kinetic complexity is avoidable, and the wide potential range scan as in the case of cyclic voltammograms [1] is not required needed to obtain the potential inversion. One disadvantage is that, if reduction products are deposited on the electrode surface and they behave as an insulating layer or an electron-transfer mediation layer, the steady-state current-potential curve would be largely distorted. However, the absence of the deposition problem can be verified by ER method using the same electrode material.

(iii) We used ER methods at a macroscopic Au electrode. The ER signal is the ac change of the reflectance of monochromatic light synchronized to the ac potential modulation with an inevitable phase delay [18]. The spectrum of the ER signal (ER spectrum) enables us to see the presence of adsorbed species or deposited film formation, if any, on the electrode surface. Without these on-surface species, the ER spectrum principally shows a difference absorption spectrum between reduced and oxidized forms in solution [18,19]. Because the oxidized form of viologen in aqueous solution has no light absorption at the wavelength longer than 350 nm

[3], we can exclusively see the absorption spectrum of the reduced forms at the electrode|solution interface.

In this paper, we first briefly review the model behind the relationship between microscopic and macroscopic redox potentials for the case of two-equivalent redox sites in a molecule. Then, we used the UME voltammetric data to obtain the potential inversion and supporting experimental data, and finally discuss electrochemistry of bis-viologen in light of present work and previous reports.

The question to be asked in this work is how much the values of $E_1 - E_2$ are for the amine terminated bis-viologen compounds in Scheme 1. High water-solubility would exclude side effects of agglomeration of the reduction product upon the measurements. At neutral pH, the terminal amine groups are in the protonated ammonium forms, between which electrostatic repulsion emerges. This can discount the intermolecular attractive interaction between $V^{\bullet+}$ sites but not so seriously, because the propyl chain between viologen unit and terminal group is long enough to escape from the intermolecular repulsion without much cost.

2. Model behind

Fig. 1.

A brief description is given herein for the two-consecutive one-electron transfer processes of a molecule with initially equivalent two redox sites using a representation in Fig. 1. Site-specific redox potentials, in other words, microscopic redox potentials, are ε_i with i = 1 to 4. For example, we write,

$$E = \varepsilon_1 + \frac{RT}{F} ln \frac{[\mathrm{B_{OO}}]}{[\mathrm{B_{OR}}]} \quad (1)$$

The subscripts to B express the oxidation state of each site. If the molecule is symmetrical, B_{OR} and B_{RO} are indistinguishable from each other, and then $\varepsilon_1 = \varepsilon_2$ and $\varepsilon_3 = \varepsilon_4$. This is the case of bis-viologen used in this work. When neither intermolecular nor intramolecular interaction emerges, $\varepsilon_1 = \varepsilon_4$ and $\varepsilon_2 = \varepsilon_3$. Under full redox equilibrium condition for all four redox processes, the concentration of 2-electron reduced form $[B_{RR}]$ can be written using the concentration of fully oxidized form $[B_{OO}]$ as a function of the electrode potential E:

$$[B_{RR}] = [B_{OO}]\exp[-f(2E - \varepsilon_1 - \varepsilon_3)] = [B_{OO}]\exp[-f(2E - \varepsilon_2 - \varepsilon_4)] \quad (2)$$

with $f = F/RT$, revealing that $\varepsilon_1 + \varepsilon_3 = \varepsilon_2 + \varepsilon_4$ always holds.

Now, macroscopic redox potentials E_1 and E_2 are given as follows.

$$E = E_1 + \frac{RT}{F} ln \frac{[B_{OO}]}{[B_{OR}] + [B_{RO}]} = E_1 + \frac{RT}{F} ln \frac{[B_{OO}]}{[B_1]}$$

$$E_1 = \varepsilon_1 + \frac{1}{f} ln2 \quad \text{when } \varepsilon_1 = \varepsilon_2 \quad (3)$$

and

$$E = E_2 + \frac{RT}{F} ln \frac{[B_{OR}] + [B_{RO}]}{[B_{RR}]} = E_2 + \frac{RT}{F} ln \frac{[B_1]}{[B_{RR}]}$$

$$E_2 = \varepsilon_2 - \frac{1}{f} ln2 \quad \text{when } \varepsilon_3 = \varepsilon_4 \quad (4)$$

where we wrote $[B_{OR}] + [B_{RO}] = [B_1]$, because B_{OR} and B_{RO} are indistinguishable for a symmetric bis-viologen. It turns out that when $\varepsilon_1 = \varepsilon_2 = \varepsilon_3 = \varepsilon_4$,

$$E_1 - E_2 = 35.62 \text{ mV at } 25℃ \quad (5)$$

When repulsive interaction between two viologen units emerges, more negative potential is needed to inject second electron to B_1 species. This is equivalent to the case that $\varepsilon_1 > \varepsilon_3$. What follows is $E_1 - E_2 > 35.62$ mV at 25℃. On the other hand, when attractive interaction emerges,

$\varepsilon_1 < \varepsilon_3$ and $E_1 - E_2 < 35.62$ mV at 25℃. Strong attraction results in $E_1 < E_2$, the inversion of the two redox potentials. The strong attraction limit gives rise to one voltammetric wave which, if the response is electrochemically reversible, represents Nernstian response with $n_{app} = 2$ (n_{app} is the number of electrons appearing in the Nernst equation).

These E_1 and E_2 are redox potentials accessible by voltammetric measurements. The case of non-interacting sites as in Eq. (5) was first discussed by Flanagan and coworkers in 1978 [20] with extension of more-than-two sites. The voltammetric wave was modeled and formulated for various $E_1 - E_2$ by Richardson and Taube in 1981 [1] by extending the simple two-consecutive electron transfer treatment by Myres and Shain in 1969 [21].

Under the steady state condition in which the bulk concentration of B_{OO} is constant, being c^*, and the bulk concentrations of B_1 and B_{RR} are zero, the surface concentrations of B_{OO}, B_1, and B_{RR} are in redox equilibrium at an electrode potential of E, and the diffusion layer thickness is a constant independent of time, the flux balance of all three species are established, provided that the diffusion coefficient of B_{OO}, B_1, and B_{RR} are the same, the steady state cathodic current $i_s(E)$ is described as

$$i_s(E) = -kAc^*\xi(E) \tag{6}$$

where

$$\xi(E) = \frac{\exp[-f(E-E_1)] + 2\exp[-f(2E-E_1-E_2)]}{1+\exp[-f(E-E_1)] + \exp[-f(2E-E_1-E_2)]} \tag{7}$$

and k is a constant, and A is the electrode area.

At a disk UME, which we also used in this work, the diffusion occurs in two dimensions, and the current density is not uniform across the flat circular surface. Nevertheless, when a steady state electrochemically-reversible response is obtained, it is established that the current-potential curve is exactly the same as Nernstian curve [2, 22], which is represented by Eqs. (6) and (7) above.

2. Experimental

2.1. Materials

1',1''-(ethane-1,2-diyl)bis[1-(3-ammonium-propyl)-4,4'-bipyridinium] hexabromide (V-C2-V) and 1',1''-(butane-1,4-diyl)bis[1-(3-ammonium-propyl)-4,4'-bipyridinium] hexabromide (V-C4-V) were newly synthesized in this work. Briefly, 1-(3-aminopropyl)-4-(4-pyridyl)-pyridinium dibromide (**1**) was obtained by Menshutkin reaction of 4,4'-bipyridine and 3-aminopropyl bromide at a molar ratio of 10:1 under reflux in acetonitrile, followed by reprecipitation of the crude product from its aqueous solution in acetone and by recrystallization from methanol + ethyl acetate. A large excess of compound **1** was reacted with 1,2-dibromoethane for 152 h to obtain V-C2-V or with 1,4-dibromobutane for 67 h to obtain V-C4-V at 70°C in DMSO. Both products as yellow-brown powder were repeatedly washed by methanol to completely remove raw substances and by-products. Molecular structures and purity were checked by ^{1}H NMR and elemental analysis.

Including the above syntheses, we used chemicals of reagent grade. Water was purified through a Milli-Q integral (Millipore) to a resistivity over 18 MΩ cm. Ar gas was of over 99.998% purity.

2.2. *UV-vis absorption spectroscopy*

The absorption spectra of buffered aqueous solutions of the two bis-viologens were measured at various concentrations employing JASCO V670DS double-beam spectrophotometer. A quartz cuvette with a light path length of 10.0 mm was used. The absorption spectra of the reduced forms were recorded in the presence of an excess of sodium dithionite.

2.3. Electrochemical measurements

A macroscopic poly-crystalline Au disk electrode (surface area: A = 0.020 cm^2) with a PEEK sheath purchased from BAS Inc. was polished by alumina slurries of down to 0.03 μm to a mirror finish. A Au disk UME of a diameter of 12.04 μm (A = 1.14 × 10^{-6} cm^2), purchased from BAS Inc. was used after polishing in the same way as the microscopic one. A Ag|AgCl electrode in saturated KCl solution served as a reference electrode, and a coiled Au wire served as a counter electrode. In all the electrochemical experiments, the Ar gas was bubbled in the solution to remove dissolved oxygen before the measurements and was continuously

flowed over the solution during the measurement. The base solution for all the electrochemical and spectroelectrochemical measurements were 50 mM phosphate buffer (from potassium salts) at pH = 7.0. The temperature for all the measurements was 23 ± 2°C. An electrochemical glass cell with an optical window was used. We employed a potentiostat HECS-315B (Huso) or HECS-9094 (Huso) with a head box 972-1 nA unit (HUSO), a digital scope DL-708E (Yokogawa), and a X-Y recorder.

2.4. Electroreflectance (ER) measurements

The details of the instrumentation and measurement procedures are described elsewhere [18,19,23]. Briefly, steady state monochromatic light was irradiated to the electrode surface, the potential of which was modulated by a sinusoidal wave. Detailed measurement parameters are found in the caption of Fig. 4. The ac change of the reflected light intensity relative to the dc intensity was monitored by a lock-in amplifier (EG&G 5210) to obtain both real and imaginary parts of the ER signal. The incident angle of the non-polarized light was 32º at the electrode|solution interface. The detector of the light intensity is a photomultiplier (R928, Hamamatsu) driven by the power suppled from a high voltage standard (Matsusada).

2.5. Potential step chrono-amperometry and chrono-reflectometory

Simultaneous recording of the transients of reflectance of monochromatic visible light and current were made, using the same setup for ER measurements, in response to a potential step. Incident light intensity and high voltage applied to the R928 photomultiplier were adjusted to obtain ca. 1 V output from the amplifier. Then, ca. 1 V was offset from the signal in order to detect only the change of the reflected light intensity in response to the potential step. To enhance the S/N ratio without any influence of the long-term decay of the signal, the data were cumulated 16 times and linearly averaged with long enough intervals between the potential steps to achieve the restoration of the initial state for each step. The digital recording of the signal was made at 10^4 sample points per second.

3. Results and Discussion

3.1. Cyclic Voltammograms

Cyclic voltammograms (CVs) for V-C4-V at the macroscopic Au electrode showed diffusion controlled reversible redox response at the potential sweep rate (v) lower than 100 mV s^{-1} with a peak separation (ΔE_p) of 32 mV when the concentration of V-C4-V (c_4) is 191 μM (Fig. 2-a) and ΔE_p = 35 mV when c_4 = 19.8 μM (Fig. 2-b). The midpoint potential, E_m, was -491 mV ± 2 mV. The absence of concentration dependence of ΔE_p and E_m together with the proportionality of the peak currents to $v^{1/2}$ indicates that observed is only the redox reaction of solution species without deposition of the reduced forms. As being also confirmed by ER measurement (*vide infra*), contribution from adsorbed species was not found. Above mentioned values of ΔE_p correspond to the Nernstian behavior with n_{app} of 1.60-1.78.

Fig. 2

CVs for V-C2-V at a concentration, c_2, of 233 μM, showed almost reversible response (Fig. 2-c) with the peak currents proportional to $v^{1/2}$ in the range of 10 – 200 mV s^{-1}. The value of ΔE_p was 94 mV, indicating that $E_1 > E_2$. As being also confirmed by ER measurement (*vide infra*), contribution from adsorbed species was not found. The midpoint potential was -460 mV, being 31 mV more positive than that of V-C4-V.

The relationship between E_1 - E_2 and apparent ΔE_p of reversible CV reported by Richardson and Taube [1] allowed us to estimate E_1- E_2 of ca. -65 ± 15 mV for V-C4-V and ca. 66 mV for V-C2-V. As pointed out by Richardson and Taube [1], ΔE_p of the CV is affected by the cathodic turn-round potential unless it is over 250 mV more negative than the cathodic peak potential, E_{pc}. In the case of viologen, such a negative turn-round potential results in the formation of neutral two-electron reduced state of viologen (V^0) giving complex waveform impossible to be analyzed. Because the turn-round potentials were only ca. 150 mV more negative than E_{pc} in our measurements, $E_{pc} - E_{p/2}$ method [1,21], where $E_{p/2}$ is the potential at the half height of the cathodic peak, may give a more reliable estimate of E_1 - E_2. We made a unified plot of the relationship between (E_1 - E_2) and ($E_{pc} - E_{p/2}$) taken from refs. 1 and 21. This was used as a measure to find E_1 - E_2 from experimental $E_{pc} - E_{p/2}$. For V-C4-V, the value of $E_{pc} - E_{p/2}$ = 35 mV at 10-30 mV/s corresponds to E_1 - E_2 = -31 mV. For V-C2-V, the

value of $E_{pc} - E_{p/2}$ = 90 mV at 10 mV/s corresponds to E_1 - E_2 = 70 mV. These results demonstrated sharp contrast of two viologens; V-C4-V exhibits strong attraction, whereas V-C2-V does repulsion. To have more precise determination of E_1 - E_2, we await the steady state UME voltammogram which does not invoke solution resistance compensation protocol.

3.2. UV-vis absorption spectrum

Fig. 3-a shows the comparison of UV-vis absorption spectra of reduced V-C4-V and V-C2-V solutions of 40 μM. V-C4-V exhibited only the spectral features of $V^{\bullet+}$ dimer with no trace of the coexistence of $V^{\bullet+}$ monomer. In contrast, V-C2-V exhibited only the features of $V^{\bullet+}$ monomer. The peak wavelengths of 357 and 859 nm are characteristic to $V^{\bullet+}$ dimer, while those at 399 and 598 nm are to $V^{\bullet+}$ monomer [3,17].

Fig. 3

For both bis-viologens, absorption spectra were measured in the concentration range from 2 μM to 40 μM. Fig. 3-b shows concentration dependent spectra for reduced form of V-C4-V. The peak position of 859.4 nm was invariant with the concentration, indicating that, at least up to 40 μM, further stacking than dimer does not take place. The absorbance values were proportional to c_4 at all the wavelengths. Even at the lowest test concentration 2.35 μM, coexistence of monomer is not seen. Concentration independent spectral structures for both viologens exclude the intermolecular association below 40 μM

3.3. Electroreflectance spectrum

Fig. 4

Fig. 4 shows ER spectra measured for the same runs as in Fig. 2. All three spectra exhibited a difference absorption spectral feature, indicating that the spectral shape represents the absorption spectrum of reduced form in the solution [18,19]. The ER spectra for V-C4-V were measured with different c_4 (Fig. 4-a and 4-b). In the UV-vis absorption spectrum, peaks at 538 nm and 859 nm originated from dimer absorption in the solution of reduced V-C4-V (Fig. 3). In the ER spectra of V-C4-V, peaks at 534 nm and 862 nm were well in accord with the dimer absorption maximum wavelengths. Because even a hump was not seen around 600 nm at c_4 = 191 μM, the presence of monomer $V^{\bullet+}$ was not detected (Fig. 4-a). The UV region ER peak was observed at 370 nm as a sharp peak because of dimer absorption, although it was not observable in Fig. 3 because of overlapping absorption of excess dithionite. Even when potential modulation of 164 Hz was used (not shown here), the presence of monomer $V^{\bullet+}$ was not detected. In the time scale corresponding to the modulation frequency up to 164 Hz, that is shorter than 6 ms, electro-generated $V^{\bullet+}$ immediately dimerizes upon the reduction elementary process of V^{2+} to $V^{\bullet+}$. Taken together, the ER spectrum of V-C4-V at c_4 = 191 μM is fully ascribable to $V^{\bullet+}$ dimer absorption.

At c_4 = 19.8 μM (Fig. 4-b), the real part showed a small positive-going peak at 401 nm and a small hump at 605 nm, although the imaginary part did not. These responses were not detected at higher concentrations (Fig. 4-a). Recalling that the real part is the in-phase component to the ac potential modulation, whereas the imaginary part is 90º out-of-phase component [18], the minor responses at 401 nm and 605 nm are attributable to a small amount of $V^{\bullet+}$ monomer of very short lifetime. In fact, these responses appeared relatively greater in the ER spectrum of 164 Hz modulation, supporting the above attribution. This $V^{\bullet+}$ monomer species is not necessarily of solution phase one but possibly of a small amount of adsorbed one, which cannot form $V^{\bullet+}$ dimer. At c_4 = 19.8 μM, such a minor species was shed light because of less solution absorption at this low c_4. Nevertheless, the predominant reduction product of V-C4-V is $V^{\bullet+}$ dimer even at low concentrations. Note that we also obtained ER voltammograms at both c_4 (not shown here), exhibiting only a single symmetric bell-shaped peak. This ensures that the surface confined species, if any, did not give detectable distortion of the response of solution redox reaction.

The ER spectrum for V-C2-V (Fig. 4-c) was measured with a high concentration to facilitate the dimerization of $V^{\bullet+}$ if possible. The ER spectrum, however, showed only two

peaks at 400 nm and 600 nm, both are the absorption maximum wavelengths of $V^{\bullet+}$ monomer. The 400 nm ER peak for V-C2-V was broader than 370 nm ER peak for V-C4-V. At this concentration, fully reduced V-C2-V (namely, $V^{\bullet+}$-C2-$V^{\bullet+}$) does not form even an intermolecular dimer, either intramolecular one. ER voltammograms (not shown here) did not exhibit additional response of viologen on the solution phase response.

Both the UV-vis absorption and ER spectra for V-C4-V revealed that, in light of spectra in literatures [3, 4, 7, 12-15, 24], $V^{\bullet+}$ formed a π-stacked face-to-face coplanar dimer without irreversible formation of new covalent bond between the two $V^{\bullet+}$ units. The $V^{\bullet+}$ dimer is known to have a structure that two moieties bipyridinium radical cation is flat (with a zero dihedral angle and negligible bending) with no mutual rotation (usually less than 5º between the longitudinal axes) and no sliding [3, 12, 13]. The intramolecular $V^{\bullet+}$ dimer in a bis-viologen molecule with a short alkyl link may have a little distorted face-to-face structure. But several reports based on the DFT calculations claimed that the distortion, if any, is rather inconsiderable so that the distortion never results in the decrease of attractive interaction energy [12, 14, 24].

3.4. Steady state voltammogram at UME

Fig. 5 shows steady state voltammograms obtained at a Au UME. For both bis-viologen, anodic and cathodic scans showed superimposable steady state current-potential curves at $v \leq$ 10 mV s^{-1}. Scanning to more negative potentials than -0.63 V was avoided to prevent the wave from becoming complex because of the occurrence of reduction to V^0, which may deposit on the electrode surface. The voltammetric curves unchanged after multiple sweeps. The measured current as a function of E, $i_{mes}(E)$, is written

$$i_{mes}(E) = pE + q + i_s(E) = pE + q + r\xi(E) \quad (8)$$

from Eqs. (6) and (7) with an additional term, $pE + q$, to represent non-zero residual background current, which is assumed to be linear to E. The experimentally obtained data were fitted to Eq. (8) using the least squares regression analysis, where p, q, r, E_1, E_2 are the parameters to fit. We set $p = 0$ for V-C4-V. As the results, we found:

E_1 = -546 (±3) mV, E_2 = -430 (±3) mV for V-C4-V ($E_1 - E_2$ = -116 mV) (9)

E_1 = -423 (±1) mV, E_2 = -486 mV (±1) for V-C2-V ($E_1 - E_2$ = +63 mV) (10)

Fig. 5

The inversion of 116 mV for V-C4-V reveals that strong attractive interaction works because of dimerization of $V^{\bullet+}$ units and that the dimerization reaches equilibrium in a shorter time compared to the time scale of the voltammetric measurements. In contrast, E_1 - E_2 = 63 mV for V-C2-V, being greater than 36 mV (see Eq. (5)), suggests that repulsive interaction works between the two units so that the first reduction makes the acceptance of the second electron more difficult than the first one. These results will be discussed in 3.6.

3.5. Simultaneous measurements of charge and reflectance in time domain

The difference of absorption spectrum between $V^{\bullet+}$-monomer and $V^{\bullet+}$-dimer is significant (Fig. 3). The ER signal exhibits the difference absorption spectrum of the redox states (Fig. 4). These facts inspired us to track the short time correlation between reflectance signals of two characteristic wavelengths. The correlation should reveal the time domain needed to establish intramolecular monomer-dimer equilibrium in V-C4-V at the close proximity of the electrode surface. We conducted simultaneous measurements of transients of charge and monochromatic light reflectance at two wavelengths, 602 nm of $V^{\bullet+}$ monomer absorption maximum and 534 nm of $V^{\bullet+}$ dimer absorption maximum, after a potential step. The potential step used was from -0.381 V to -0.641 V. At each wavelength, 16 step transients for averaging were linearly cumulated with an interval time of over 10 s.

The current transients obtained in the measurements at 602 and 534 nm gave rise to the same Cottrell slope, ensuring that the drift of the system was negligible between the two sets of measurements at different wavelengths. Fig. 6 shows the correlation between the relative change of reflectance at 602 nm (ΔR_{602nm}) and that at 534 nm (ΔR_{534nm}) after the step for a

period of 1 s. The deviation from the (0, 0) point originates from the way of experimental recording of the reflected light allowing an arbitrary but constant off-set. The plot shows a linear correlation after 5 ms. The equilibrium with predominant existence of $V^{\bullet+}$ dimer reached before 5 ms has passed since the potential step. This fact enabled us to conclude that the intramolecular dimerization upon accepting the second electron is much faster than the time scale of our electrochemical control used in this work except for the period of 5 ms just after the potential step. These results are in line with the fact that the ER spectrum (Fig. 4) for V-C4-V showed negligible or only a small amount of $V^{\bullet+}$ monomer. The period of 5 ms is approximately the time needed for double-layer charging.

Fig. 6

3.6. Discussion on redox processes and redox potentials

To our best knowledge, the redox potential inversion of V-C4-V, $E_1 - E_2$ = -116 mV, is the largest value among those ever being evaluated for the bis-viologen family. For V-C2-V, we obtained $E_1 - E_2$ = 63 mV, exhibiting repulsive interaction. The in-total 2-electron reduction of bis-viologen should decrease the intramolecular electrostatic repulsion between V^{2+} sites. Therefore, the main origin of observed repulsion may be electronic through the ethane-1,2-diyl linkage. We will approach this point in future using DFT-based calculation. The fact that no dimerization of V-C2-V was observed also supports that dimerization of V-C4-V is the intramolecular-type, although V-C4-V has nearly the same size as V-C2-V and the same charge.

Derozier and coworkers estimated $E_1 - E_2 \approx$ -60 mV in water for butane-1,4-diyl bis-viologen with -CH_3 outer deviations [5]. They also reported $E_1 - E_2$ = 20 mV in DMF and $E_1 - E_2 \approx$ -50 mV (i.e. inversion) in water. In contrast to our work, they used CH_3-V-C4-V-CH_3, which may have less electrostatic repulsion when forming intramolecular dimer. The value of $E_1 - E_2$ was not able to be obtained for CH_3-V-C2-V-CH_3 because of solubility obstacle of its reduced form [5]. In contrast, we used hexa-cationic starting molecule, overcoming the obstacle, and eventually we obtained $E_1 - E_2$ of 63 mV, revealing

the repulsive interaction, that is, $\varepsilon_3 < \varepsilon_1$. Note that similar repulsive interaction was observed in DMF [5]. Mohammed investigated three bis-viologen molecules at a glassy carbon electrode in acetonitrile [6]. Although attractive interactions are observed, it is not as much as to induce redox potential inversion. Neta and coworkers reported $E_1 - E_2$ = -78 mV for ortho-xylene-linked bis-viologen in water [7]. Significant solvent dependence indicates that the electrostatic repulsion of the viologen sites as well as solvation energy are sharp functions of the solvent properties; dimerization must overcome the electrostatic repulsion, and it is known that desolvation of water is significant upon reduction. In the case of the ferrocene pivot with two equivalent viologen sites with alkyne or phenyl rigid linker in DMSO, $E_1 - E_2$ = 15 mV [12]. For the bisporphyrin pacman-like molecular tweezer driven by propyl linked bis-viologen in DMF, $E_1 - E_2$ = 1 mV [14]. Kannappan and coworkers reported a value of $E_1 - E_2$ = -27 mV for a propane-1,3-diyl bis-viologen in acetonitrile [24].

Neta and coworkers made a thorough investigation on the intramolecular association of bis-viologens in water, using voltammetric measurements and pulse radiolysis [7]. They represented the tendency to form intramolecular dimers thermodynamically using the equilibrium constant of disproportionation:

$$R\text{-}V^{2+}\text{-}V^{\bullet+}\text{-}R + R\text{-}V^{2+}\text{-}V^{\bullet+}\text{-}R \rightarrow R\text{-}V^{2+}\text{-}V^{2+}\text{-}R + R\text{-}V^{\bullet+}\text{-}V^{\bullet+}\text{-}R \quad (11)$$

They also mentioned that the progress of this process is of microsecond order.

Turning our eyes to the change of ionic charge upon redox reaction, recall that the terminal groups of the bis-viologen in this work at pH = 7.0 are in the form of ammonium cation, a single molecule EE process is written as:

$$(\text{bis-}V^{2+})^{6+} \xrightarrow[+\ e^-\ (\text{electrode})]{} (V^{2+}\text{-}V^{\bullet+})^{5+} \xrightarrow[+\ e^-\ (\text{electrode})]{} (\text{bis-}V^{\bullet+})^{4+} \quad (12)$$

where the total molecular ionic charge was put as the superscript to the bracket. The disproportionation process of Eq. (11) is rewritten with the total molecular charge superscript as:

$$2(V^{2+}\text{-}V^{\bullet+})^{5+} \rightarrow (\text{bis-}V^{\bullet+})^{4+} + (\text{bis-}V^{2+})^{6+} \quad (13)$$

We have no experimental implication which processes above is predominant in the proximity of the electrode surface, a unimolecular process of Eq. (12) or a bimolecular one of Eq. (13), because these two are thermodynamically equivalent and are indistinguishable in the time scale of our experiments. The disproportionation process of Eq. (13), however, requires the collision of 5+ cations of the mutual average distance of 20 nm in the solution of 200 μM. Both large electrostatic repulsion to be overcome and large potential inversion in the case of V-C4-V may make the unimolecular EE process be predominant.

Fig. 7

Taken together, the fractions of the bis-viologen species are depicted in Fig. 7 as a function of the electrode potential relative to E_m. The presence of V^{2+}-C4-$V^{\bullet+}$ is minor, whereas V^{2+}-C2-$V^{\bullet+}$ is the majority species in the 63 mV of interval. Applying Eqs. (3) and (4) for the symmetric bis-viologens, we obtain $\varepsilon_3 = \varepsilon_1 + 152$ mV for V-C4-V and $\varepsilon_3 = \varepsilon_1 - 27$ mV for V-C2-V. This indicates that the attractive interaction energy in the redox process of V-C4-V, 152 meV, corresponds to 5.9 k_BT at 25°C, where k_B is the Boltzmann constant. In addition to the enthalpy term of stacking, the entropy term may contribute largely, because reduction is accompanied by partial desolvation. When more circumjacent water molecules should be removed upon dimerization, entropy may have a larger contribution. The dimerization Gibbs free energy of methyl viologen diiodide in aqueous solution at room temperature is reported to be -16.37 kJ mol^{-1} [3,25], which is equal to -5.9 k_BT. This value is apparently the same as the interaction energy of V-C4-V. Although consideration of the partial free energy for curling the C4 alkyl chain linker and the electronic interaction energy between $V^{\bullet+}$ and V^{2+} through the C4 linker needed, the C4 linker did not obstruct the intramolecular dimerization at least.

In addition to the details of the interaction energy, a new question may arise whether an intramolecular pre-stacking structure formation for $V^{\bullet+}$-C4-V^{2+}, a dimer precursor with

attractive intermolecular $V^{\bullet+}\cdots V^{2+}$ interaction, can take place or not. A calculation approach is now setup in our laboratory.

4. Conclusions

Redox reactions of highly water-soluble bis-viologens with alkane-1,*n*-diyl (n = 2 and 4) linkage were investigated at Au electrodes using ultra-micro electrode steady state voltammetry and electroreflectance methods in addition to conventional voltammetry. The redox potential inversion for the bis-viologen with a butane-1,4-diyl linkage (V-C4-V) between the two viologen units was evaluated to be 116 mV ($E_1 - E_2$ = -116 mV). In contrast, the bis-viologen with an ethane-1,2-diyl linkage (V-C2-V) has the second potential 63 mV more negative than the first ($E_1 - E_2$ = 63 mV), exhibiting no dimerization below 0.2 mM. Because V-C2-V, whose intramolecular dimerization of $V^{\bullet+}$ units is sterically prohibited, did not show even the intermolecular dimerization at concentrations below 0.2 mM, the dimerization of V-C4-V should be exclusively of the intramolecular type. In this work, we used both-end-NH_3^+ terminated symmetrical bis-viologens. Its high water-solubility provided a clear-cut analysis of the redox process. In addition, highly charged states, hexa-cationic V^{2+}–V^{2+} and tetra-cationic $V^{\bullet+}$–$V^{\bullet+}$, may effectively annihilate bimolecular stacking. This was also confirmed spectrophotomerically. The value of $E_1 - E_2$ = -116 mV corresponds to the attractive interaction energy in the redox process of 5.9 k_BT; this value is apparently the same as the dimerization Gibbs free energy of methyl viologen in water.

Acknowledgements

The authors acknowledge with appreciation to Drs. Bun Chan and Hironobu Tahara at Nagasaki University for technical advices and useful discussions, and Dr. Tomohiro Higashi (presently at The University of Tokyo) for his help on synthesis. This work was supported by a Grant-in-Aid (to TS) for Scientific Research on Innovative Area “Molecular Robotics” (No. 24104004) of The Ministry of Education, Culture, Sports, Science, and Technology, Japan and Ogasawara Science Foundation (to TS).

References

[1] D.E. Richardson, H. Taube, Determination of E_2^0-E_1^0 in multistep charge transfer by stationary-electrode pulse and cyclic voltammetry: application to binuclear ruthenium ammines, Inorg. Chem., 20 (4) (1981) 1278-1285.
http://doi.org/10.1021/ic50218a062

[2] A.J. Bard, L.R. Faulkner, Electrochemical Methods – Fundamentals and Applications, , 2nd Ed., John-Wiley & Sons, New York, 2001, Chaps. 5 and 12.

[3] P.M.S. Monk, The Viologens, John-Wiley & Sons, Chichester, 1998, Chap. 3 and 6.

[4] M. Furue, S. Nozakura, Photoreduction of bisviologen compounds, viologen-$(CH_2)_n$-viologen, by 2-propanol, Bull. Chem. Soc. Jpn., 55 (2) (1982) 513-516.
https://doi.org/10.1246/bcsj.55.513

[5] A. Deronzier, B. Galland, M. Vieira, Electrochemical behavior of some paraquat dimer molecules. A potential direct bielectronic mediating system, Nouv. J. de Chimie, 6 (1982) 97-100.
https://doi.org/???????

[6] M. Mohammad, Cyclic voltammetric studies on some multicentre bipyridilium compounds, Electrochim. Acta, 33 (3) (1988) 417-419.
https://doi.org/10.1016/0013-4686(88)85037-0

[7] P. Neta, M.-C. Richoux, A. Harriman, Intramolecular association of covalently linked viologen radicals, J. Chem. Soc., Faraday Trans. 81 (1985) 1427-1443.
http://doi.org/10.1039/F29858101427

[8] S.K. Lee, S.Y. Shin, S. Lee, C. Lee, J.W. Park, Conformation and binding properties of polymethylene-linked bisviologens–2-naphthol complexes, J. Chem. Soc., Perkin Trans. 2 (10) (2001) 1983-1988.
http://doi.org/10.1039/B102858H

[9] T. Sagara, Y. Fujihara, T. Tada, Molecular Structure Dependence of the Phase Transition Spike Response of Viologens at an HOPG Electrode Using Bisviologen and Carboxylated Viologen, J. Electrochem. Soc., 152 (2005) E239-E246.
http://doi.org/10.1149/1.1939127

[10] N. Asakura, R. Goto, T. Kamachi, I. Okura, Electron transfer from hydrophobic porphyrin to hydrophilic viologen via the photoexcited singlet state in water, Chem. Lett. 38 (12) (2009) 1200-1201.
http://doi.org/10.1246/cl.2009.1200
[11] G. Casellaza, G. Saielli, DFT study of the interaction free energy of π– π complexes of fullerenes with buckybowls and viologen dimers, New J. Chem., 35 (7) (2011) 1453-459.
http://doi.org/10.1039/C1NJ20117D
[12] A. Iordache, M. Oltean, A. Milet, F. Thomas, B. Baptiste, E. aint-Aman, C. Bucher, Redox control of rotary motions in ferrocene-based elemental ball bearings, J. Am. Chem. Soc. 134 (5) (2012) 2653-671.
https://doi.org/10.1021/ja209766e
[13] M. Bonchio, M. Carraro, G. Casella, V. Causin, F. Rastrellib, G. Saielli, Thermal behaviour and electrochemical properties of bis(trifluoromethanesulfonyl)amide and dodecatungstosilicate viologen dimers, Phys. Chem. Chem. Phys., 14 (8) (2012) 2710-2717.
http://doi.org/10.1039/C2CP23580C.
[14] A. Iordache, M. Retegan, F. Thomas, G. Royal, E. Saint-Aman, C. Bucher, Redox-Responsive Porphyrin-Based Molecular Tweezers, Chem. Eur. J., 18 (25) (2012) 7648 -7653.
http://doi.org/10.1002/chem.201200842
[15] K. Wadhwa, S. Nuryyeva, A. C. Fahrenbach, M. Elhabiri, C. Platas-Iglesias, A. Trabolsi, Intramolecular redox-induced dimerization in a viologen dendrimer, J. Mater. Chem. C, 1 (12) (2013) 2302-2307.
http://doi.org/10.1039/C3TC00740E
[16] R.J. Alvarado, J. Mukherjee, E.J. Pacsial, D. Alexander, F.M. Raymo, Self-assembling bipyridinium multilayers, J. Phys. Chem. B, 109 (13) (2005) 6164-6173.
http://doi.org/10.1021/jp044797i
[17] C. Gao, S. Silvi, X. Ma, H. Tian, A. Credi, M. Venturi, Chiral supramolecular switches based on (R) - binaphthalene-bipyridinium guests and cucurbituril hosts, Chem. Eur. J., 18 (52) (2012) 16911-16921.
http://doi.org/10.1002/chem.201202378

[18] T. Sagara, UV-visible Reflectance Spectroscopy of Thin Organic Films at Electrode Surface, In Advances in Electrochemical Science and Engineering, Volume 9: "In situ Spectroscopic and Diffraction Methods", Eds. C. Alkire, D. M. Kolb, J. Lipkowski, P. N. Ross, Wiley-VCH Verlag, GmbH, Weinheim, pp. 47-95 (2006).

[19] T. Sagara, H. Murase, N. Nakashima, Frequency Dependence of the Electroreflectance Signal for Redox Reaction of Solution-Phase Species at the Electrode Surface: Formulation and Experimental Verification, J. Electroanal. Chem., 454 (1-2) (1998), 75-82. https://doi.org/10.1016/S0022-0728(98)00232-0

[20] J.B. Flanagan, S. Margel, A.J. Bard, F.C. Anson, Electron transfer to and from molecules containing multiple, noninteracting redox centers. Electrochemical oxidation of poly(vinylferrocene), J. Am. Chem. Soc., 100 (13) (1978) 4248-4253. http://doi.org/10.1021/ja00481a040

[21] R.L. Myers, I. Shain, Determination of E_2^0 - E_1^0, for overlapping waves in stationary electrode polarography, Anal. Chem., 41 (7) (1969) 980. http://doi.org/10.1021/ac60276a011

[22] C.G. Zoski, In Modern Techniques in Electroanalysis, Ed. P. Vanỳsek, Chemical Analysis Series, Vol. 139, John Wiley & Sons, 1996, Chap. 6, pp. 242-312.

[23] T. Sagara, K. Izumi, Electroreflectance study of potential dependent phase changes of dodecyl sulfate adlayer on a Au(111) Electrode, Electrochim. Acta, 162 (2015) 4-10. https://doi.org/10.1016/j.electacta.2014.10.109

[24] R. Kannappan, C. Bucher, E. Saint-Aman, J.-C. Moutet, A. Milet, M. Oltean, E. Métay, S. Pellet-Rostaing, M. Lemairec, C. Chaixd, Viologen-based redox-switchable anion-binding receptors, New J. Chem., 34 (7) (2010) 1373-1386. https://doi.org/10.1039/B9NJ00757A

[25] E.M. Kozower, J.L. Cotter, Stable Free Radicals. II. The Reduction of 1-Methyl-4-cyanopyridinium Ion to Methylviologen Cation Radical, J. Am. Chem. Soc., 86 (24) (1964) 5524-5527. https://doi.org/10.1021/ja01078a026

Figure Captions

Scheme 1. Bis-viologen compounds used in this work.

Fig. 1. Schematic model of redox equilibria for a molecule bearing two redox sites: B_{ij} represents oxidation state, ε_k is the microscopic redox potential.

Fig. 2. Cyclic voltammograms (CVs) at a macroscopic poly-Au electrode in the solution of (a) 191 μM V-C4-V, (b) 19.8 μM V-C4-V, (c) 233 μM V-C2-V. The base electrolyte solution was 50 mM phosphate buffer (pH = 7.0). For (a) through (c), v values in the left-hand-side CVs are 50, 70, 100, 150, and 200 mV s^{-1}, and v values in the right-hand-side CVs are 10, 20, 30, and 50 mV s^{-1}.

Fig. 3. UV-vis absorption spectra of the solutions of V-C4-V and V-C2-V. Concentrations are given in the figure. Measurement conditions are described in the experimental section.

Fig. 4. Electroreflectance spectra obtained at a macroscopic Au electrode in the solutions of bis-viologen at the formal potentials obtained from CV. Potential modulation frequency, 14 Hz, modulation amplitude (zero-to-peak), 19.8 mV. (a) V-C4-V, c_2 = 191 μM; (b) V-C4-V, c_4 = 19.8 μM; (c) V-C2-V, c_2 = 233 μM.

Fig. 5. Steady state voltammograms of (a) V-C4-V (191 μM) and (b) V-C2-V (233 μM) at the Au-UME with v = 2 mV s^{-1}. Circles are the data points used for the least squares fitting calculations, while original continuous voltammetric curves are not shown here. Red thin lines are the best fit results (R = 0.99996 for (a) and R = 0.9997 for (b)). The best fit parameters other than those given in the text were: (a) q = 0.00022±0.00053, r = -0.2272±0.0004, (b) p = 0.0680±0.0244, q = 0.0224±0.0078, r = -0.1965±0.0037.

Fig. 6. Representation of correlation dc reflectance changes (as a transient response to a potential step from -0.381V to -0.641 V) between 602 nm and 534 nm measured in 191 μM V-C4-V aqueous solution at a macroscopic poly-Au electrode. Linear averaging after

accumulation of 16 repeated steps were made with long enough interval time period (at least 10 s re-equilibration at the initial potential).

Fig. 7. Potential diagram of the fractions of bis-viologen species for V-C4-V (a) and V-C2-V (b) depicted based on $E_1 - E_2$.

Graphical Abstract

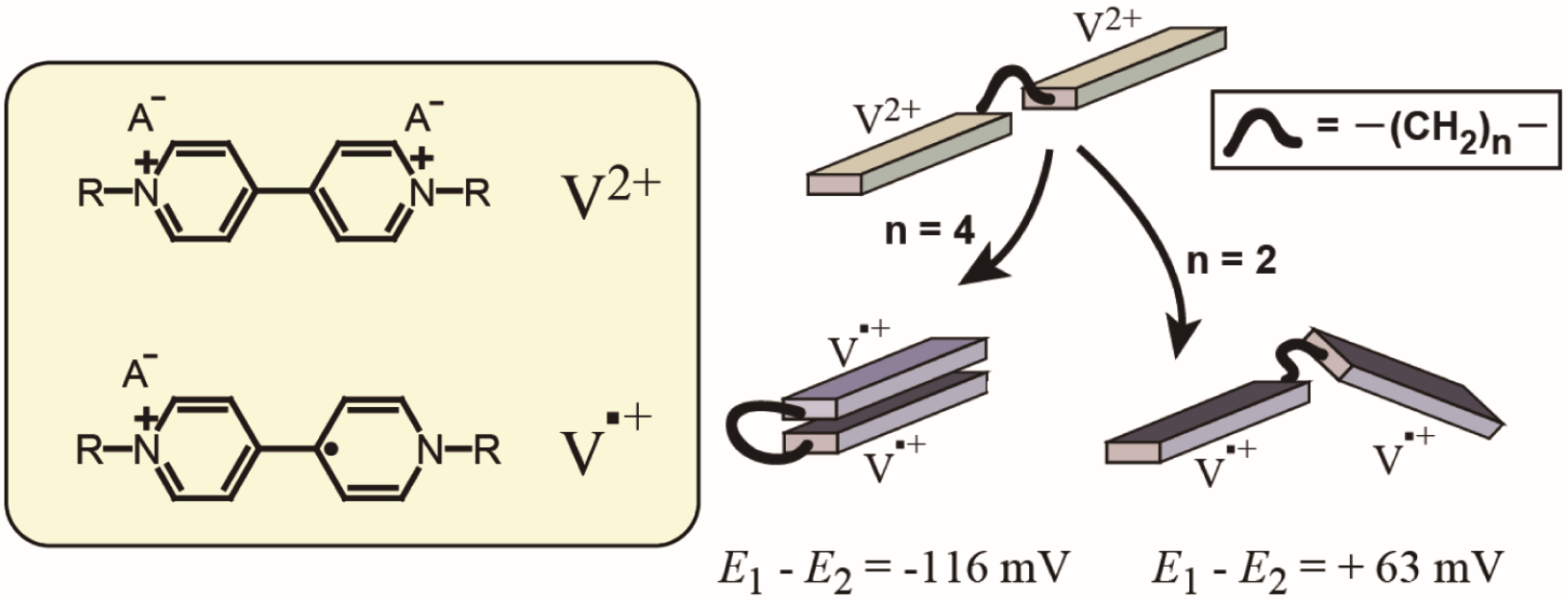

Scheme 1

V-C2-V

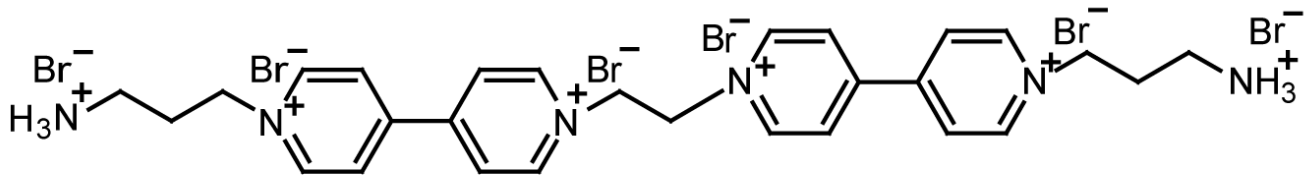

V-C4-V

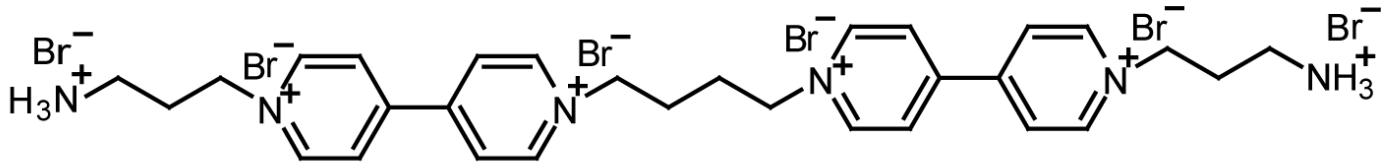

Fig. 1

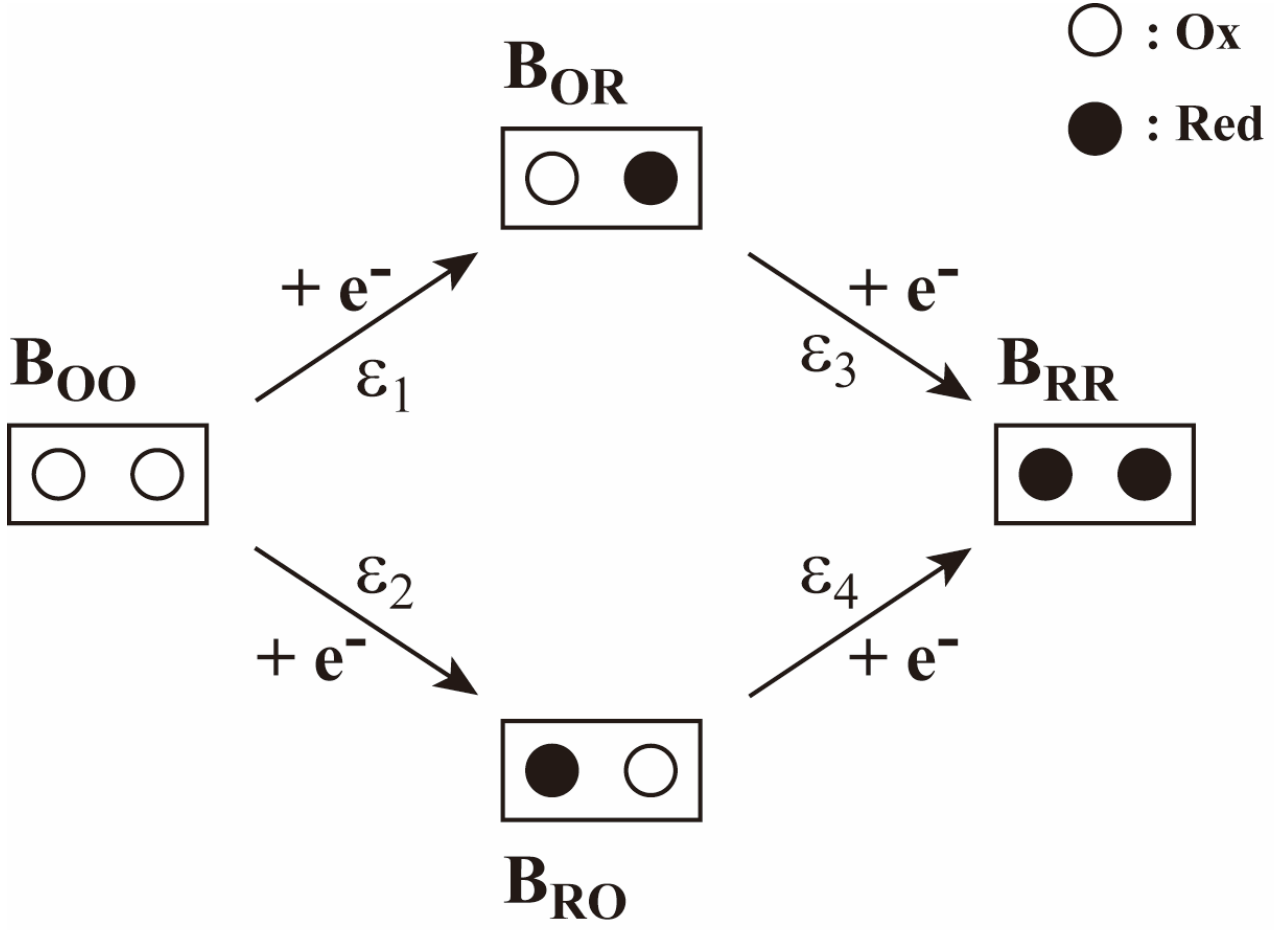
○ : Ox
● : Red
B_{OR}
B_{OO}
B_{RR}
B_{RO}
+ e⁻
ε_1
+ e⁻
ε_3
ε_2
+ e⁻
ε_4
+ e⁻

Fig. 2

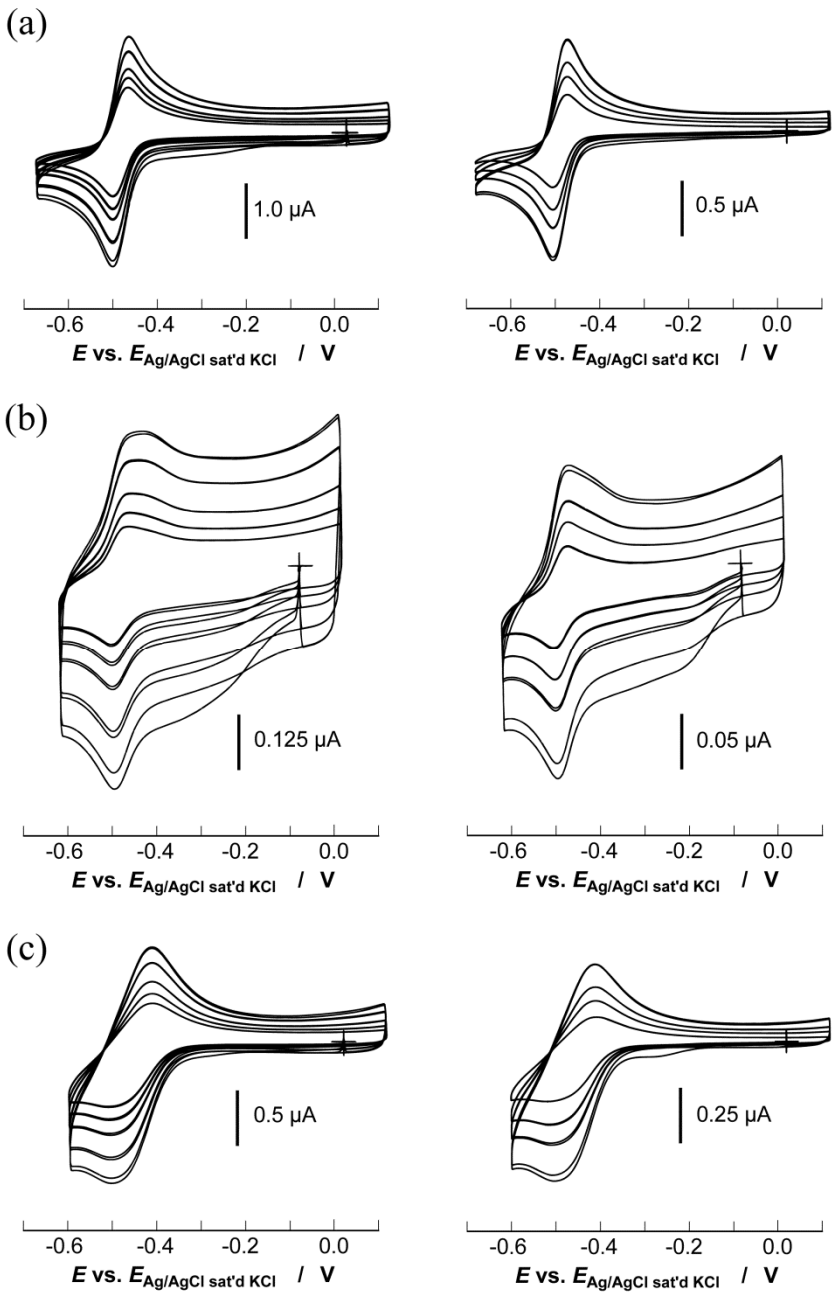
(a)
1.0 μA
0.5 μA
-0.6 -0.4 -0.2 0.0
E vs. E Ag/AgCl sat'd KCl / V
(b)
0.125 μA
0.05 μA
-0.6 -0.4 -0.2 0.0
E vs. E Ag/AgCl sat'd KCl / V
(c)
0.5 μA
0.25 μA
-0.6 -0.4 -0.2 0.0
E vs. E Ag/AgCl sat'd KCl / V

Fig .3

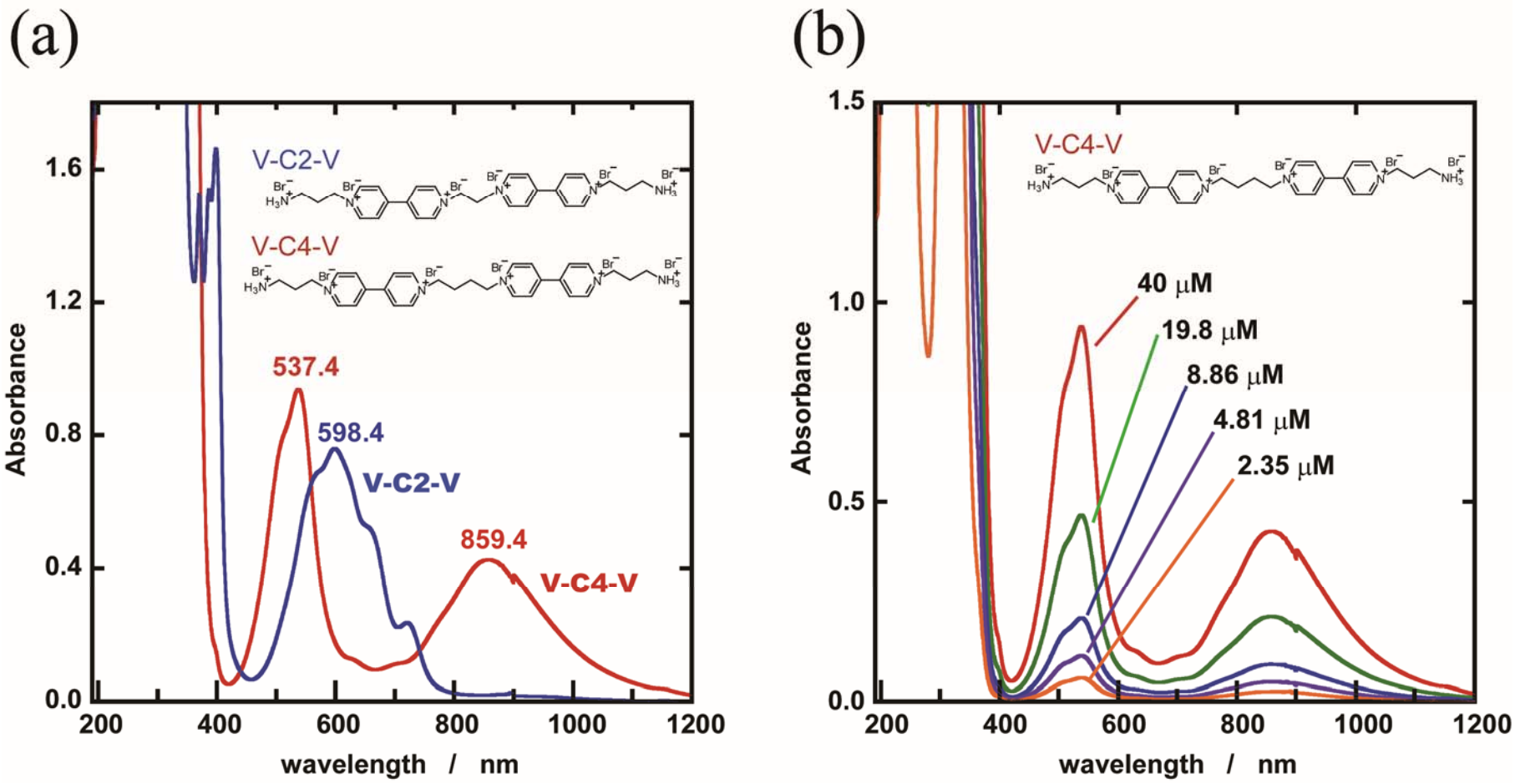
(a)
V-C2-V
V-C4-V
537.4
598.4
V-C2-V
859.4
V-C4-V
Absorbance
wavelength / nm
(b)
V-C4-V
40 μM
19.8 μM
8.86 μM
4.81 μM
2.35 μM
Absorbance
wavelength / nm

Fig. 4

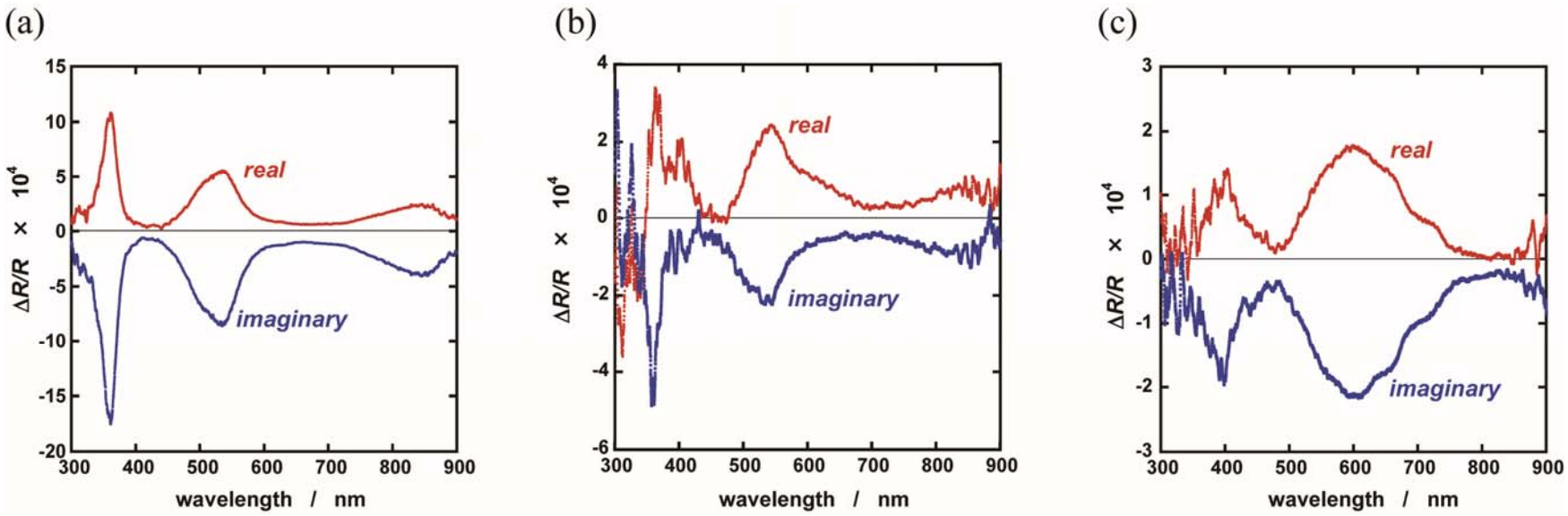

Fig. 5

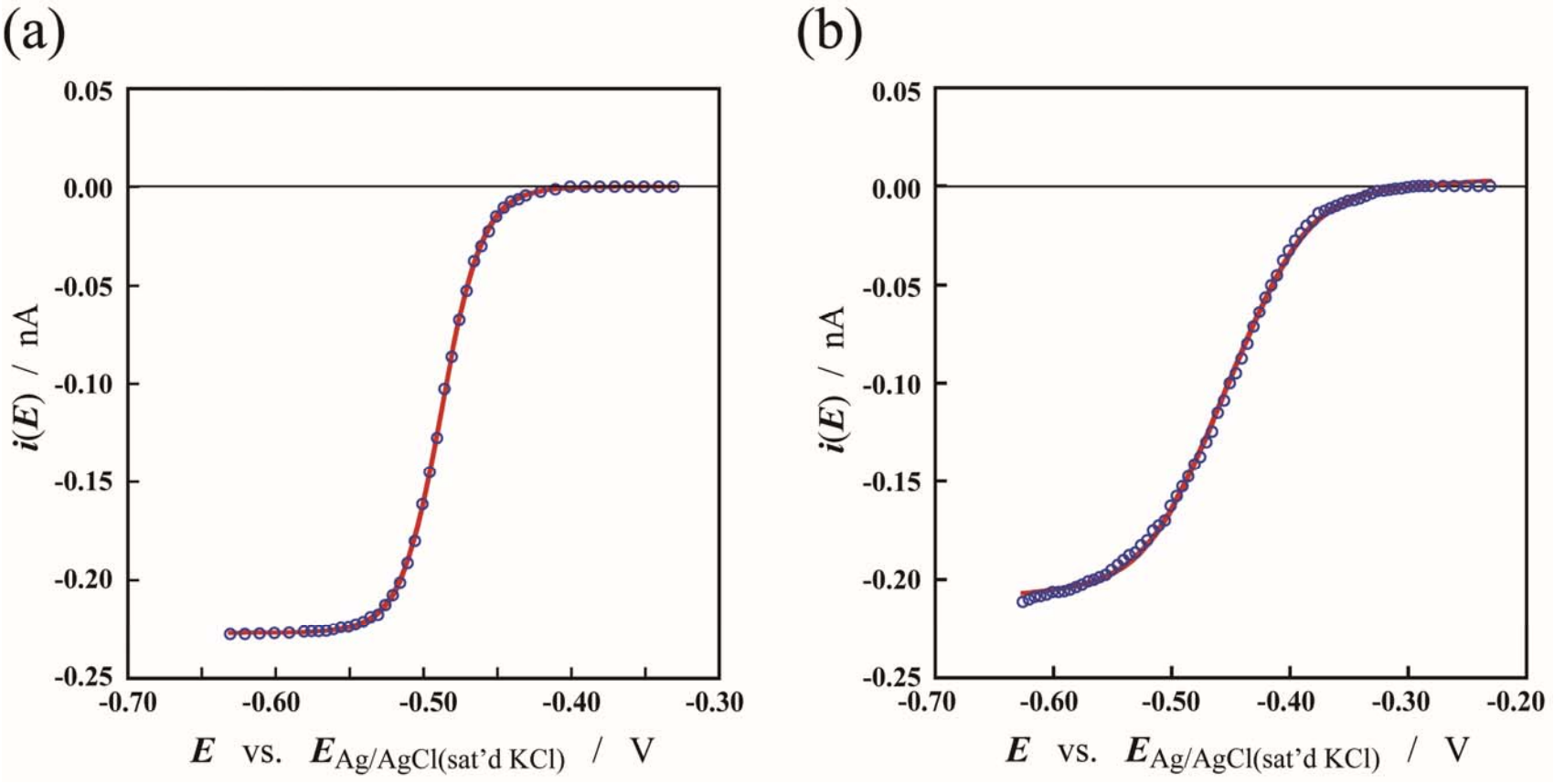
(a)
0.05
0.00
-0.05
-0.10
-0.15
-0.20
-0.25
i(E) / nA
-0.70
-0.60
-0.50
-0.40
-0.30
E vs. E Ag/AgCl(sat'd KCl) / V
(b)
0.05
0.00
-0.05
-0.10
-0.15
-0.20
-0.25
i(E) / nA
-0.70
-0.60
-0.50
-0.40
-0.30
-0.20
E vs. E Ag/AgCl(sat'd KCl) / V

Fig. 6

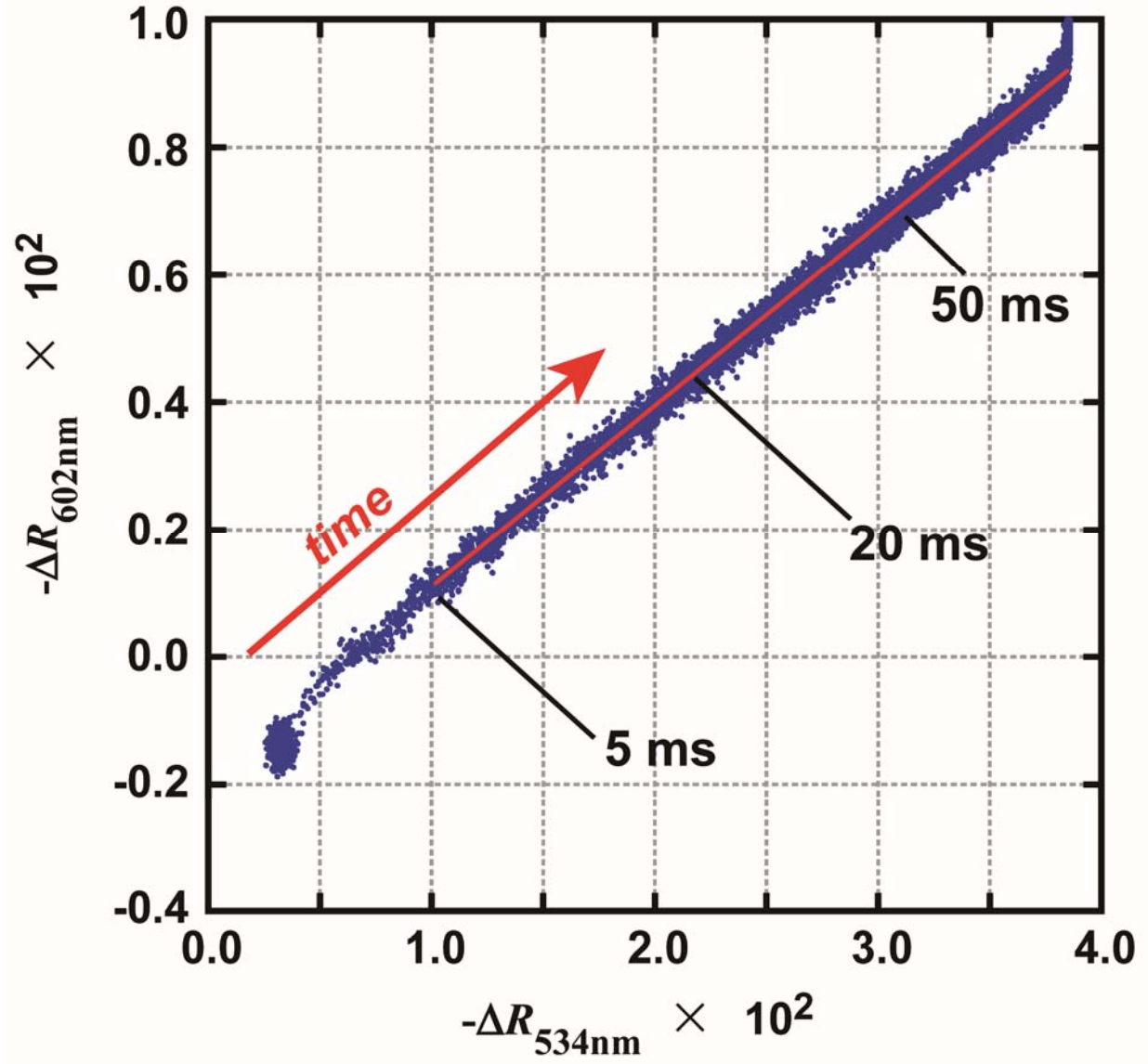
1.0
0.8
0.6
0.4
0.2
0.0
-0.2
-0.4
0.0
1.0
2.0
3.0
4.0
$-\Delta R_{602nm} \times 10^2$
$-\Delta R_{534nm} \times 10^2$
time
50 ms
20 ms
5 ms

Fig. 7